Deep-Sea Research II 57 (2010) 1098–1110

Contents lists available at ScienceDirect

Deep-Sea Research II

journal homepage: www.elsevier.com/locate/dsr2

Eddy-mean flow interaction in the decadally modulating Kuroshio Extension system

Bo Qiu *, Shuiming Chen

Department of Oceanography, University of Hawaii at Manoa, Honolulu, HI, USA

ARTICLE INFO

Article history:
Received 6 July 2008
Accepted 28 November 2008
Available online 11 January 2010

Keywords:
Kuroshio Extension
Decadal variability
Eddy-mean flow interaction
Recirculation gyre

ABSTRACT

Satellite altimeter sea-surface height (SSH) data of the past 16 years are used to investigate the decadal changes of the Kuroshio Extension (KE) system that oscillated between a stable and an unstable dynamic state. During the stable state of 10/1992–06/1995 and 01/2002–12/2004, the KE jet was intense and had a northerly zonal mean path and a well-defined southern recirculation gyre. During the unstable state of 07/1995–12/2001 and 01/2005–present, the KE jet had a reduced eastward transport and a more southerly flow path. Transitions between the two dynamic states are caused by the basin-scale wind-stress curl forcing in the eastern North Pacific related to the Pacific decadal oscillations (PDOs) or the North Pacific Gyre Oscillations (NPGOs). During the positive PDO (or negative NPGO) phase, the intensified Aleutian Low generates negative SSH anomalies in the eastern North Pacific through Ekman divergence. As these wind-induced negative SSH anomalies propagate to the west as baroclinic Rossby waves, they weaken the zonal KE jet and shift its path southward. As its path is pushed southward ($\sim 32^{\circ}$N), the deep-reaching KE jet has to ride over the shallow Shatsky Rise, generating localized disturbances that lead to their subsequent development along the KE jet west of the Shatsky Rise. The sequence opposite to that listed above occurs when the PDO (NPGO) changes to its negative (positive) phase. After the KE system transitions from a stable to unstable state, the enhanced eddy interaction is found to strengthen both the southern recirculation gyre and quasi-stationary meanders along the KE's upstream path. This nonlinear eddy interaction is important in determining the amplitude of the observed decadal KE variability.

1. Introduction

Accumulation of high-quality sea-surface height (SSH) data from satellite altimeters over the past 16 years has provided us not only a tool to monitor changes in the world ocean's mesoscale eddy field, but also a means to explore the relationship between the time-varying eddy signals and the background mean flow field. In the North Pacific Ocean, the highest mesoscale eddy variability is detected along the Kuroshio Extension (KE) after the Kuroshio separates from the coast of Japan near 35°N and 140°E (Fig. 1). Free from the constraint of coastal boundaries, and with its eastward transport enhanced by the neighboring recirculation gyres, the KE east of Japan has long been recognized as rich in large-amplitude meanders and energetic pinched-off eddies (e.g., Mizuno and White, 1983; Yasuda et al., 1992; Joyce et al., 2001). By taking advantage of the repeat SSH measurements from satellite altimeters, many studies in recent years have investigated the variability of the KE jet and its mesoscale eddy field (Tai and White, 1990; Qiu et al., 1991; Ichikawa and Imawaki, 1994; Adamec, 2000; Ducet and Le Traon, 2001; Ebuchi and Hanawa, 2001; Vivier et al., 2002 among others). For a comprehensive review of our improved knowledge of the KE system, the readers are referred to Qiu (2002).

One important feature increasingly clear from the longer, available SSH time series is that the level of eddy kinetic energy in the KE region undergoes a well-defined decadal modulation. The amplitude of this modulation is substantial: the eddy kinetic energy level in the "active" period can be three times as large as that in the "calm" period. The decadal modulation in the KE's mesoscale eddy field was noted in Qiu and Chen (2005) to be a manifestation of the decadal variability of the KE system that oscillated between a stable and an unstable dynamic state. The analysis of Qiu and Chen's (2005) study covered the period of October 1992—December 2004. As will be shown in this study, the KE system underwent another transition from a stable to an unstable state in late 2005. Although a similar transition took place in mid 1995, the 2005 transition was much better observed both because more satellite altimeters were in operation[1] and because several in situ observational programs, such as the

* Corresponding author.
E-mail address: bo@soest.hawaii.edu (B. Qiu).

[1] Compared to the TOPEX/Poseidon (T/P) and European Remote Sensing (ERS)-1 missions in 1995, there were four concurrent altimeter missions in 2005: T/P, Envisat, Jason-1 and Geosat Follow-On.

0967-0645/$ - see front matter © 2010 Elsevier Ltd. All rights reserved.
doi:10.1016/j.dsr2.2008.11.036

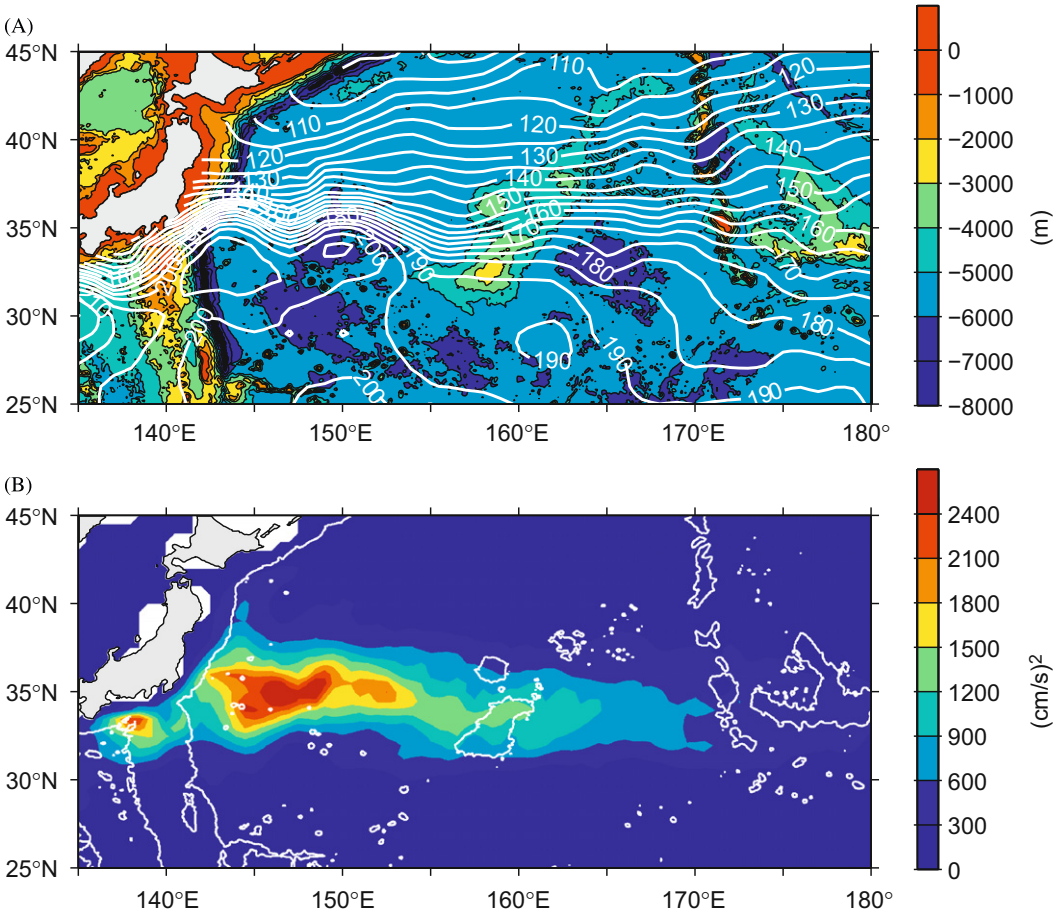

Fig. 1. (A) Mean surface dynamic height field (cm; white contours) relative to 1000 dbar from Teague et al. (1990). Colored map shows the bathymetry based on Smith and Sandwell (1994). (B) Eddy kinetic energy calculated from the satellite altimeter SSH data from October 1992 to September 2008. White contours denote the 4000-m isobaths.

International Argo program and the Kuroshio Extension System Study (KESS) program, were underway (Qiu et al., 2007).

It is important to understand the decadally modulating mesoscale eddy signals. Changes in the level of mesoscale eddies along the KE band modify the exchanges of heat, salt and other dynamical quantities, such as potential vorticity, across the KE front. Indeed, recent observational studies based on historical hydrographic and more recent KESS/Argo profiling float data indicate that an increase in the level of mesoscale eddies can significantly reduce the formation of Subtropical Mode Water through southward cross-frontal transport of the surface high-potential vorticity water (Qiu and Chen, 2006; Qiu et al., 2007). The time-varying mesoscale eddy variability can also feedback onto the background mean flow field and this topic has not been previously explored well for the KE system.

The present study has three objectives. The first is to describe the bimodal dynamic states of the KE system that includes the KE jet, the southern recirculation gyre, and their associated mesoscale eddy signals. The second objective is to clarify what controls the transitions between the different dynamic states of the KE system. To do so, we adopt a simple baroclinic Rossby model and demonstrate that the KE's dynamic state transitions are initiated by the surface wind stress curl forcing related to the Pacific decadal oscillations (PDOs; Mantua et al., 1997). Connections to the wind-stress curl forcing associated with the North Pacific Gyre Oscillations (NPGOs) identified recently by Di Lorenzo et al. (2008) will also be discussed. Our third objective is to relate the observed variations in the eddy kinetic energy level to the latitudinal migration of the KE jet due to the wind stress curl-induced SSH anomaly signals. As the intensity of mesoscale eddies modulates in time, their impact upon the mean KE circulation also changes. This change is evaluated in this study by adopting a simple dynamic framwork relating to the eddy vorticity flux convergence.

2. Observed decadally modulating KE system

For this study we use the global SSH anomaly dataset compiled by the Collocte Localisation Satellites (CLS) Space Oceanographic Division of Toulouse, France. This dataset merges the TOPEX/Poseidon, European Remote Sensing Satellite (ERS) 1/2, Geosat Follow-On (GFO), and Jason-1 along-track SSH measurements and provides improved capability for detecting mesoscale SSH signals (Le Traon et al., 1998; Ducet et al., 2000). It has a 7-day temporal resolution, a $1/3^{\circ}$-longitude Mercator spatial resolution, and covers the period from October 1992 through September 2008. From the SSH anomaly field $h'(x,y,t)$, we derive the total SSH field $h(x,y,t)$ by adding the climatological SSH field $\overline{h}(x,y)$ (see Fig. 1 A) to the anomaly field: $h=\overline{h}+h'$. For brevity, the total SSH field will be referred to simply as the SSH field throughout this study.

One effective way to describe the low-frequency variability of the KE jet is to superimpose snapshots of the KE paths in individual years (Fig. 2); here the KE paths are defined by the 170-cm SSH contours in the weekly SSH maps. As can be inferred from the mean SSH map of Fig. 1 A, the 170-cm SSH contour is located near the $\partial h/\partial y$ maxima and serves as a good indicator for the KE jet axis. In the region between the coast of Japan and the Shatsky

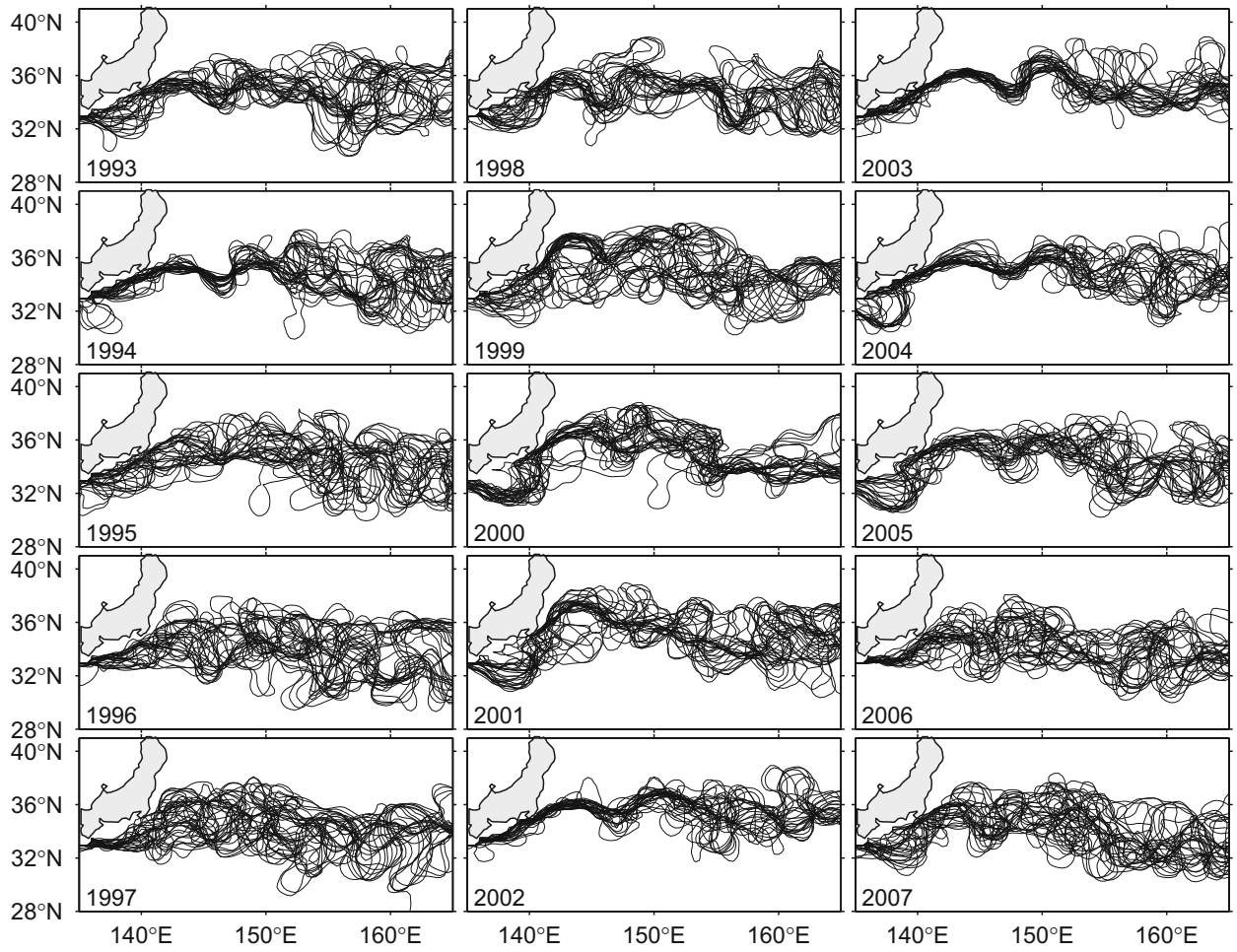

Fig. 2. Yearly paths of the Kuroshio and Kuroshio Extension defined by the 170-cm contours in the weekly SSH fields. Paths of every 14 days are plotted here.

Rise around 158°E, it is clear from Fig. 2 that the KE paths were relatively stable in 1993–1995 and 2002–2005. In contrast, spatially variable paths dominated from 1996 to 2001 and from 2006 to present.

This bimodal behavior of the KE paths is equally well illustrated in Fig. 3a, showing the time series of the path length of the KE jet integrated from 141°E to 153°E. A straight zonal path in the region would have a length of 1,090 km and a larger value in Fig. 3 A signifies a more spatially convoluted path taken by the KE jet. With better temporal resolution than the yearly maps of Fig. 2, Fig. 3 A reveals the KE jet changed from a stable to an unstable state in mid 1995 and late 2005, and the transition from the unstable to stable state took place near the end of 2001. Note that the monthly time-scale path length fluctuations seen in Fig. 3 A during the KE's unstable state reflect the shedding and merging of mesoscale eddies from/to the KE jet (for examples of these processes, see Figs. 2 and 3 in Qiu et al., 2007).

Fig. 3 B shows the time series of eddy kinetic energy level in the region of 32°−38°N and 141°−153°E. To emphasize the contribution from the mesoscale eddy signals, the eddy kinetic energy is calculated here based on the high-pass filtered h' data with timescales shorter than 300 days. Compared to Fig. 3 A, it is not surprising that changes in the eddy kinetic energy level tend to correlate with the KE path length variability; e.g., a spatially convoluted KE path tends to correspond to a higher level of regional eddy kinetic energy. Notice that the eddy kinetic energy time series of Fig. 3 B appears less clear-cut in defining the bimodal states of the KE system than the KE path length time series. This is because the eddy kinetic energy level presented in Fig. 3 B can be high due to the presence of isolated warm- or cold-core eddies translated from the east, *even* when the KE path is in a relatively stable state.

Associated with the bimodal path variations of the KE system, there is also a concurrent change in the latitudinal position of the KE jet. Fig. 3 C shows the time series of the mean latitudinal position of the KE jet averaged from 141°E to 158°E. Aside from the monthly time-scale fluctuations induced by mesoscale eddies, there exists a general tendency for the mean KE path to shift southward when the KE's dynamic state changes from a stable to unstable state; in addition, this southward shift tends to be followed by a gradual northward migration of the mean KE path.

Another important feature of the bimodal changes of the KE system is reflected in the strength of the KE's southern recirculation gyre (RG; see Fig. 3 D). Here, the strength of the RG is defined by

$$R(t) \equiv \iint_A h(x,y,t)\,dx\,dy, \tag{1}$$

where A denotes the area south of the KE jet from 141°E to 158°E within which the SSH value exceeds 2.0 m. The time series of $S(t)$ resembles the time series of the KE's latitudinal position (Fig. 3 C), indicating that the decadal strengthening/weakening of the KE's southern RG is in sync with the lateral migration of the KE's path. It is worth emphasizing that the strengthening of the RG started in 1997, *after* the KE's dynamic state changed from the earlier stable to an unstable state in mid 1995. The strengthening of the RG continued throughout the KE's remaining unstable period (i.e., 1998–2001) and it ceased in 2002–2004 after the KE system

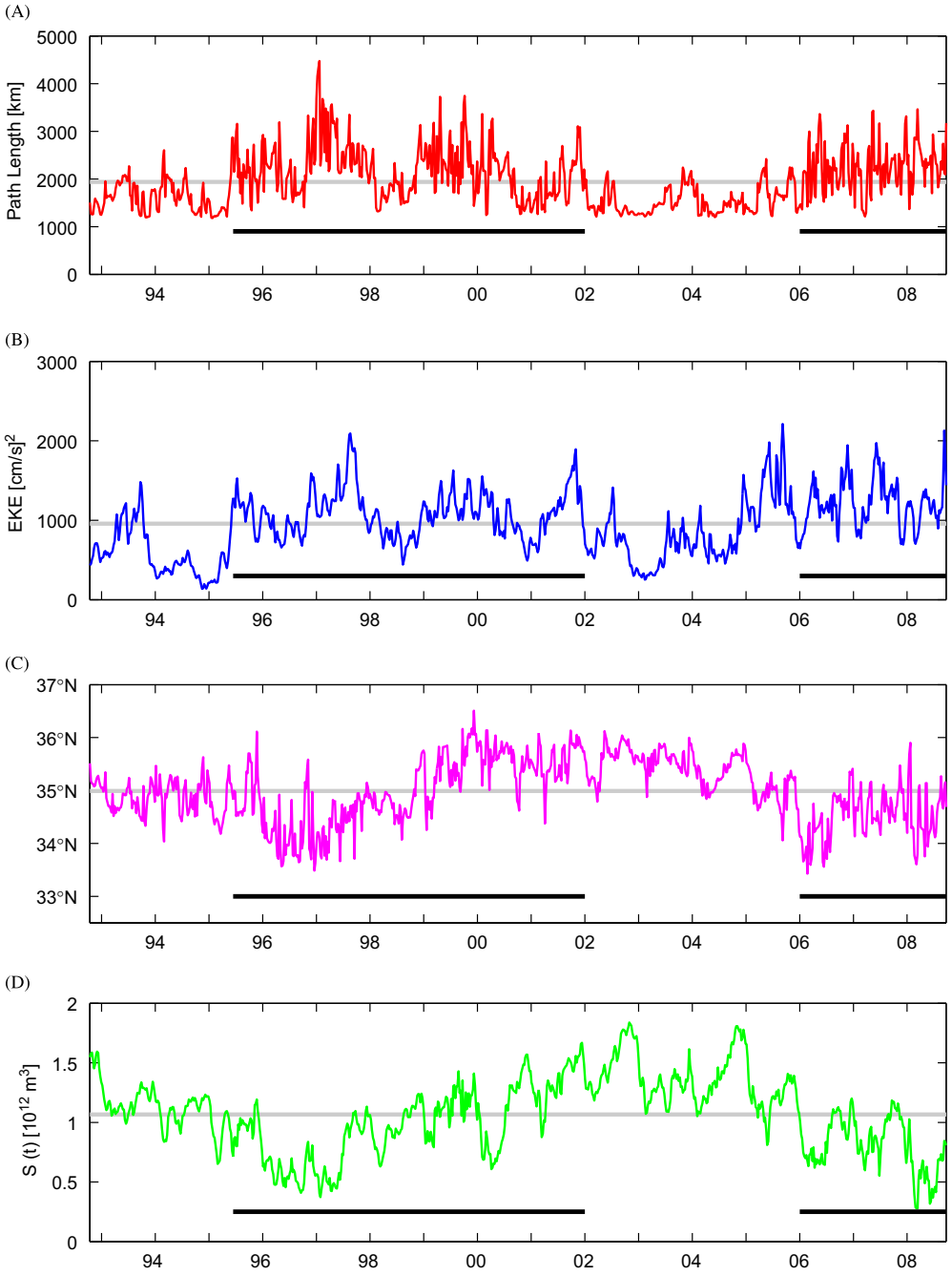

Fig. 3. (A) Upstream KE path length integrated from 141°E to 153°E. (B) Eddy kinetic energy in the upstream KE region of 32°–38°N and 141°–153°E. (C) Latitudinal position of the KE averaged from 141°E to 158°E. (D) Strength of the KE recirculation gyre defined by Eq. (1). Grey lines denote the mean values of the quantity over the period of analysis and dark lines indicate the periods when the KE system is in the unstable state.

switched back to the stable state. This issue of how the decadally modulating mesoscale eddy forcing affects the mean circulation will be addressed further in Section 4.

To provide a better look at the changes in the KE's southern RG, we plot in Fig. 4 the annually averaged SSH field over the past 15 years. As described in Fig. 3 D, the gradual, but steady, enhancement of the RG after 1998, and the weakening of the RG in the years after 1993 and 2004 can be clearly discerned in Fig. 4.

3. Forced response of the KE system

Several recent theoretical and numerical modeling studies have pointed to the importance of decadal variability of a western boundary current, such as the KE, involving self-sustained, intrinsic changes of the southern RG (e.g., Qiu and Miao, 2000; Schmeits and Dijkstra, 2001; Primeau, 2002; Hogg et al., 2005; Pierini, 2006; Berloff et al., 2007). Although the data analysis result shown in Fig. 3 D indicates a clear decadal modulation in the strength of the KE's southern RG, it is important to recognize that this decadal modulation is *not* a localized phenomenon initiated by the southern RG. To demonstrate this point, we plot in Fig. 5 the yearly averaged SSH anomaly field in the entire midlatitude North Pacific Ocean.[2] In these h' maps, strengthening

[2] In the region surrounding the KE, Fig. 5 would be the same as Fig. 4 if the mean SSH value is added to the SSH anomaly data.

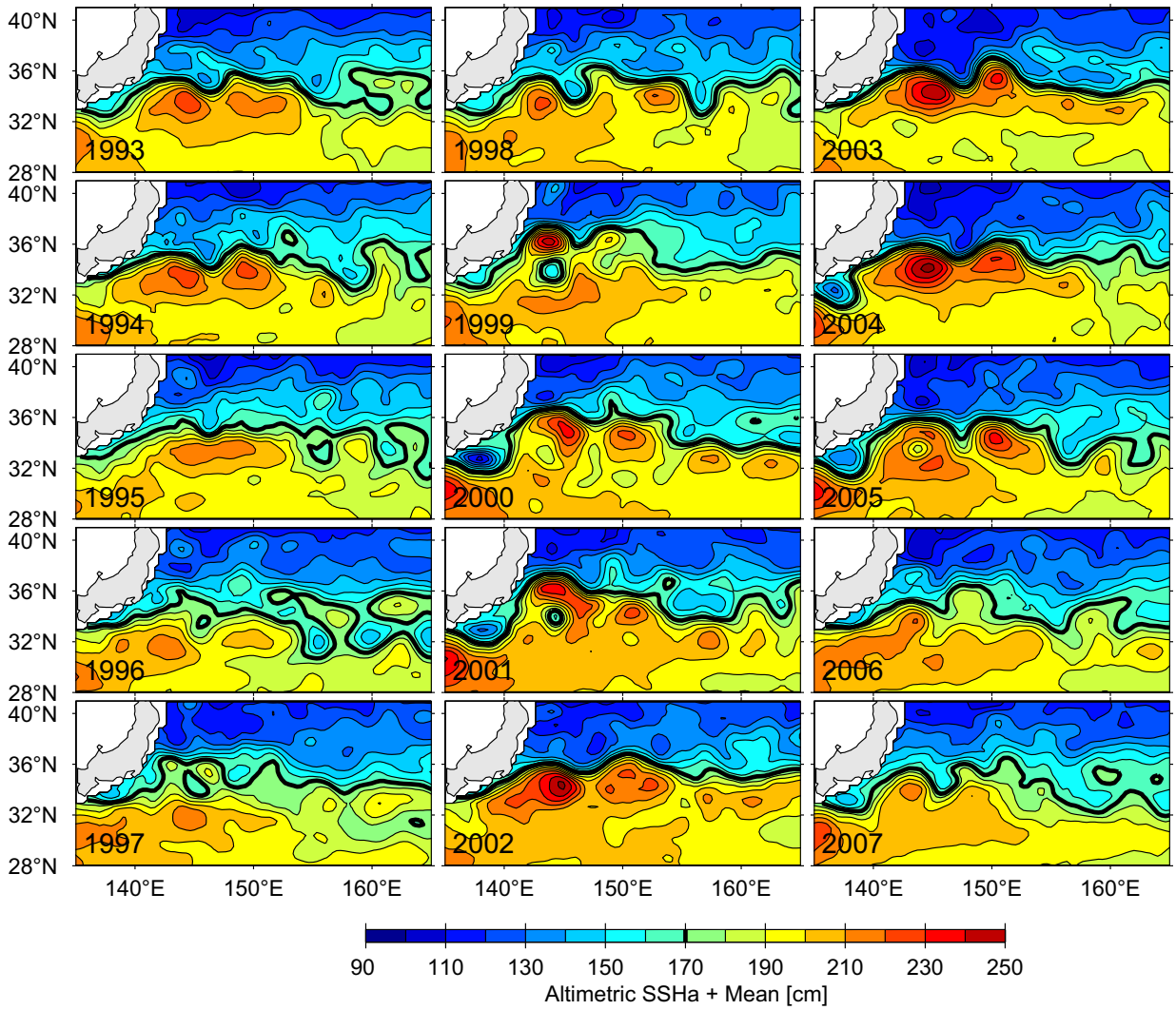

Fig. 4. Maps of yearly averaged sea-surface height field. Contour intervals are 10 cm with the thick lines denoting the 170-cm contours.

of the southern RG in 2004, for example, is reflected by the fact that the SSH value is anomalously high southeast of Japan. By stepping back in time, it is clear that this high SSH anomaly had its origin in the eastern North Pacific Ocean near 160°W around 1999. Similarly, weakening of the RG in 1997 can be traced back to the negative SSH anomalies originating in the eastern North Pacific around 1993.

The fact that the decadally varying SSH anomalies observed inside the KE's southern RG had their origin in the eastern part of the North Pacific Ocean is best seen in Fig. 6b, which shows the time-longitude plot of $h'(x,y,t)$ averaged in the latitudinal band of the southern RG: 32°−34°N. Notice that the decadal SSH changes in the eastern North Pacific Ocean can be *qualitatively* explained by the wind stress curl variability associated with the Pacific decadal oscillation (PDO) that has its center of action around 160°W (Mantua et al., 1997). Specifically, when the PDO index is positive (see Fig. 6 D), the Aleutian Low intensifies and shifts southward, and this works to generate negative SSH anomalies near 160°W in the eastern North Pacific through Ekman divergence. The opposite is true when the PDO index is negative: the wind-induced Ekman convergence in this case leads to regional, positive SSH anomalies near 160°W. Once they are generated in the eastern North Pacific Ocean, the SSH anomalies tend to propagate subsequently westward at the speed of baroclinic Rossby waves c_R; in Fig. 6 B, $c_R \simeq 3.7\,\mathrm{cm\,s^{-1}}$.

The above-mentioned connection between the PDO index (Fig. 6 D) and the SSH anomalies around 160°W (Fig. 6 B) is, of course, no more than a qualitative statement. By now, it is well established that the large-scale, wind-induced SSH variability is controlled by baroclinic Rossby wave dynamics (e.g., Miller et al., 1998; Deser et al., 1999; Seager et al., 2001; Schneider et al., 2002; Qiu, 2003; Taguchi et al., 2007). Specifically, the linear vorticity equation under the longwave approximation states:

$$\frac{\partial h'}{\partial t} - c_R \frac{\partial h'}{\partial x} = -\frac{g'\,\mathrm{curl}\,\boldsymbol{\tau}}{\rho_0 g f}, \tag{2}$$

where $h'(x,y,t)$ is the SSH anomaly, g the gravitational constant, g' the reduced gravity, ρ_0 the reference density, f the Coriolis parameter, and $\boldsymbol{\tau}$ the anomalous wind stress vector, respectively. Given the observed wind stress curl data, $h'(x,y,t)$ can be hindcast by integration along the baroclinic Rossby wave characteristic in individual y latitude:

$$h'(x,y,t) = \frac{g'}{c_R \rho_0 g f} \int_0^x \mathrm{curl}\,\boldsymbol{\tau}\left(x', y, t + \frac{x - x'}{c_R}\right) dx'. \tag{3}$$

In Eq. (3), we have ignored the solution due to the eastern boundary forcing at $x = 0$. As detailed in Fu and Qiu (2002), contribution from the eastern boundary forcing in the midlatitude North Pacific is limited to the area a few Rossby radii away from the boundary. (This may also be visually confirmed in Fig. 6 B.)

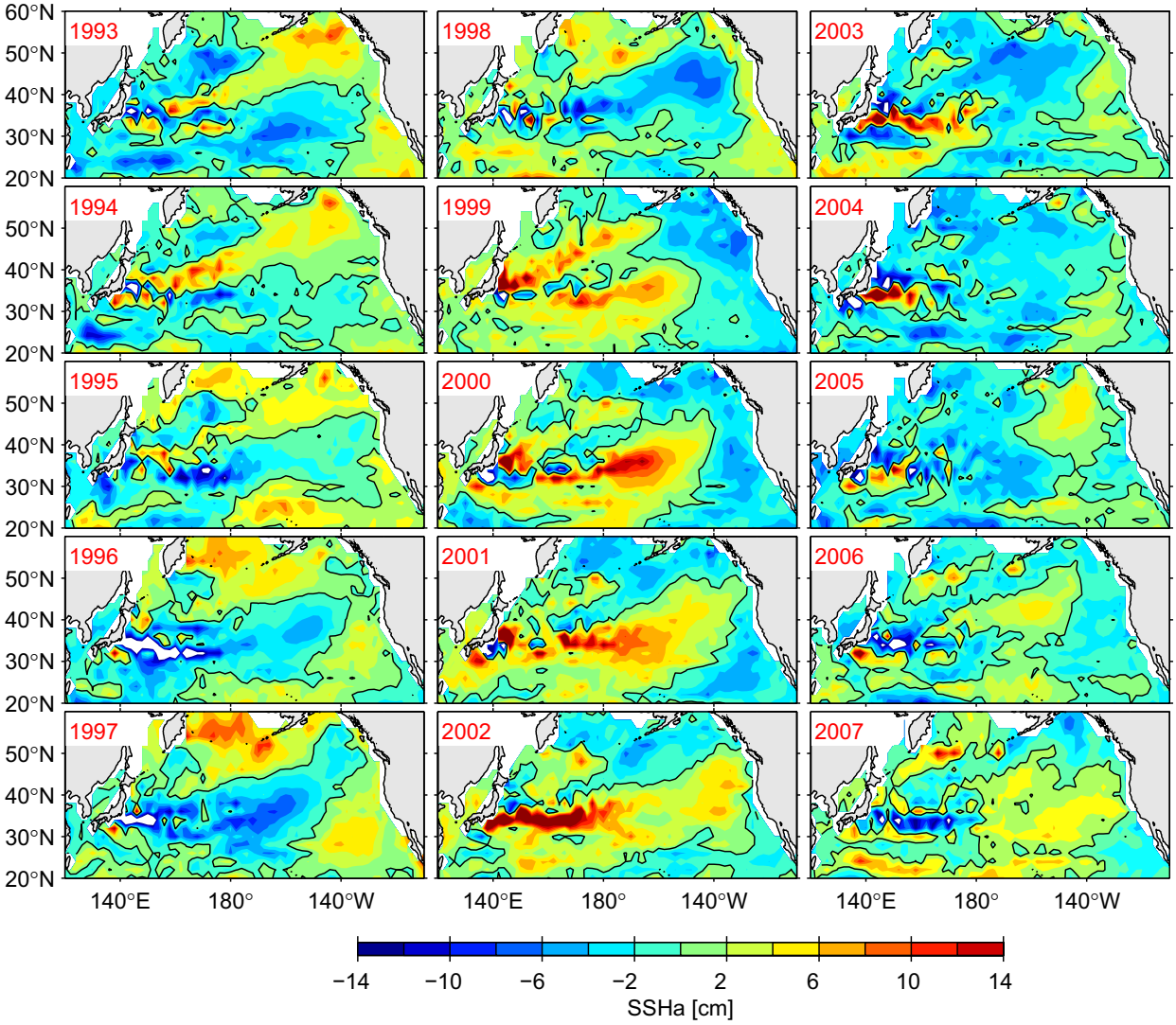

Fig. 5. Maps of yearly averaged sea-surface-height anomaly field. Zero SSH anomaly contours are highlighted by the black lines.

Fig. 6 C shows the time-longitude plot of the h' field in the $32^\circ-34^\circ$N band modeled by Eq. (3) with the use of $g' = 0.04\,\mathrm{m\,s^{-2}}$ and the monthly wind stress curl data from the National Centers for Environmental Prediction–National Center for Atmospheric Research (NCEP–NCAR) reanalysis (Kistler et al., 2001). Being the western boundary current extension in the subtropical gyre of the North Pacific Ocean, the KE jet has its associated density surfaces outcropping near 37°N. Because of this, much of the observed surface KE variability has been shown to be related to the time-varying SSH signals in this southern RG band of $32^\circ-34^\circ$N (Qiu and Chen, 2005; Taguchi et al., 2007). As expected, the Rossby wave model captures well all the large-scale SSH anomaly signals that changed signs on the decadal timescales and this includes the recent sign change in SSH occurring in 2007 in the central North Pacific Ocean around 160°W. The linear correlation coefficient between the observed and modeled h' fields is $r = 0.42$ and this coefficient increases to 0.59 when only the interannual SSH signals are retained in Fig. 6 B. This quantitative comparison confirms the notion that the decadal KE modulations detected by the satellite altimeter data over the past 16 years are initiated by the incoming SSH anomalies signals generated by the PDO-related wind forcing in the eastern North Pacific Ocean.

While we emphasized the initiation of phase changes of the KE system by the remote wind-induced SSH signals above, it is equally important to point out that the wind-driven Rossby wave model underestimates the observed SSH anomaly signals in the western North Pacific (i.e., west of the dateline). In fact, altimeter measurements reveal that the level of eddy kinetic energy in the upstream KE region of $141^\circ-153^\circ$E modulates with the incoming SSH anomalies: the eddy kinetic energy level increases when the incoming SSH anomalies are negative and vice versa (cf. Figs. 6 A and B). Such a change in characteristics of the mesoscale eddy field cannot be explained by the linear Rossby wave dynamics, Eq. (2).

At a first glance, the correspondence between a high regional eddy kinetic energy level and a *negative* SSH anomaly south of the KE jet appears paradoxical: a negative SSH anomaly south of the KE jet represents a weakened zonal KE jet and, based on the theory of baroclinic instability (Pedlosky, 1987), less mesoscale eddies might be expected in this state because of reduced instability of the KE jet. A careful look at the sequential SSH maps indicates that much of the KE path variability and the enhanced mesoscale eddy signals in the upstream KE region (i.e., west of 158°E; Fig. 1 B) originate around the Shatsky Rise. Fig. 7 A shows the SSH values averaged zonally from 162°E to 180° as a function of time and latitude. The thick black line in the figure denotes the 170-cm contour and represents in this case the zonal-mean KE jet axis downstream of the Shatsky Rise. One consistent

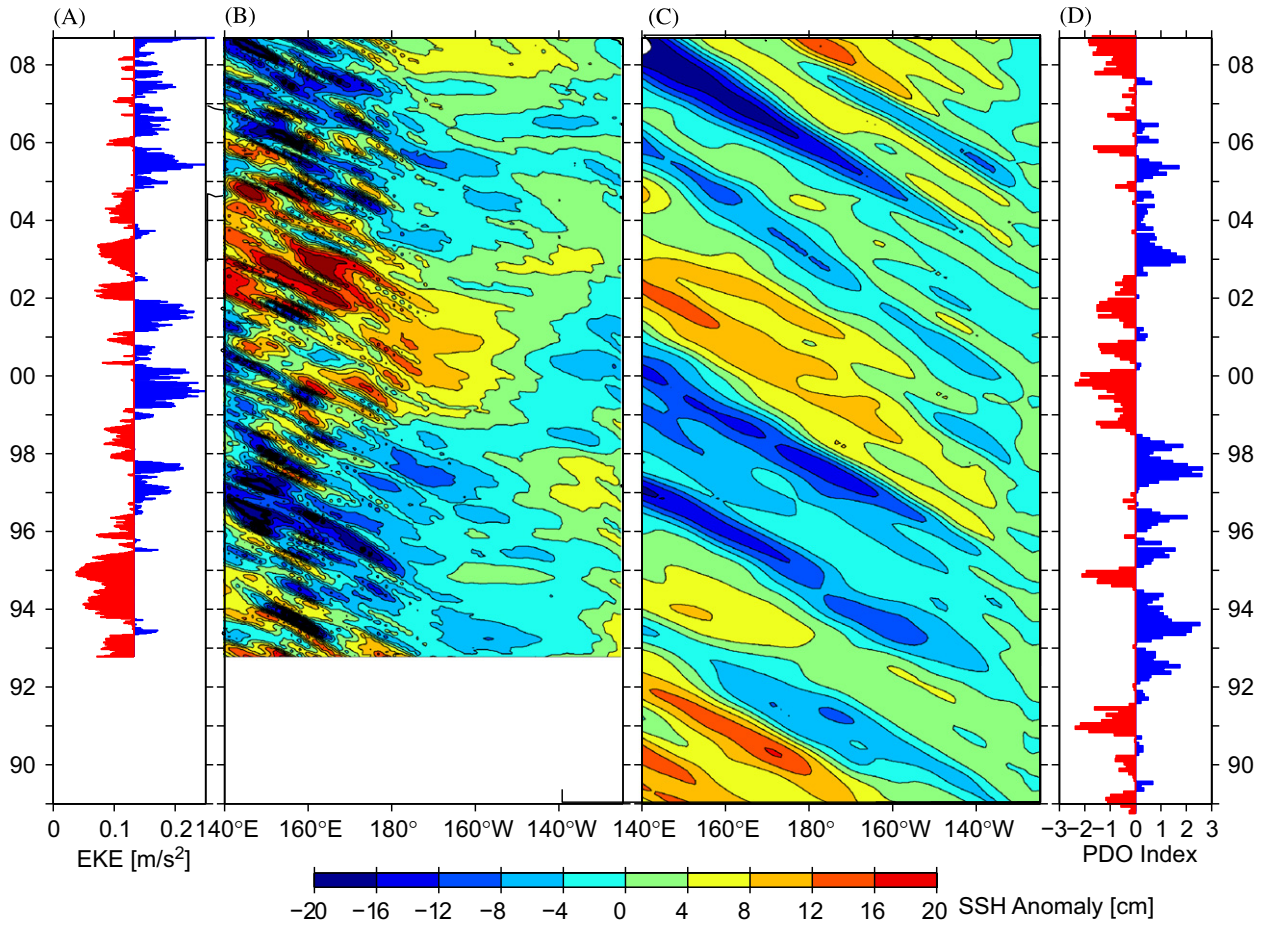

Fig. 6. (A) Time series of eddy kinetic energy (EKE) in the upstream KE region of 141°–153°E and 32°–38°N. Here, EKE is calculated using the weekly SSH anomaly data by assuming geostrophy. For comparison with the PDO index, the time series is plotted as the deviation from the regional mean EKE value. (B) SSH anomalies along the zonal band of 32°–34°N from the satellite altimeter data. (C) Same as panel b but from the wind-forced baroclinic Rossby wave model. (D) PDO index from http://jisao.washington.edu/pdo/PDO.latest.

feature occurring prior to the KE's transition from a stable to an unstable state in mid 1995 and end of 2005, is the *southward* migration of the broad-scale, downstream KE jet axis from ~35°N to ~32°N. These southward path migrations, as we discussed above, result from the incoming negative SSH anomalies generated by the positively phased PDO wind forcing in the eastern North Pacific Ocean.

The latitudinal migration of the broad-scale KE jet has a profound effect upon the stability of the upstream KE jet because of the presence of the Shatsky Rise. Along 158°E, where the Shatsky Rise is situated, Fig. 7 B shows a deep passage with depth exceeding 4,500 m exists around 35°N. This deep passage allows the northerly positioned KE jet[3] to pass over the Shatsky Rise without triggering perturbations. When the KE jet migrates southward to ~32°N, Fig. 7 B indicates that the main body of the KE jet runs into the shallow portion of the Shatsky Rise with a depth of ~2,000 m and this interaction with the shallow topography of the Shatsky Rise by the southerly KE jet provides the initial perturbations in the KE jet around 158°E. Once they are generated, these perturbations propagate westward and their subsequent interactions with the intense, upstream KE jet lead to an elevated eddy kinetic energy state of the KE system west of the Shatsky Rise.

4. Eddy's impact on the time-mean circulation

While the wind-driven Rossby wave dynamics of Eq. (2) was useful in explaining the phase transitions of the KE system, it fails, as we noted above in Figs. 6 B and C, to account for the amplitude of the SSH anomaly changes detected in the upstream KE region. Given that the level of mesoscale eddy variability can differ by three-fold in the different dynamic states of the KE system (recall Fig. 3 B), it is important to quantify the effect of the mesoscale eddies upon the time-varying mean circulation field that is, in part, modulated by the wind-driven Rossby wave dynamics. To do so, we follow Hoskins et al. (1983) and evaluate the quantity:

$$S(x,y,t) = \nabla^{-2}(-\nabla\cdot\overline{\mathbf{u}'\zeta'}), \tag{4}$$

where $\mathbf{u}' \equiv (u', v')$ is the surface anomalous velocity vector, which is related to h' geostrophically through $f\mathbf{k}\times\mathbf{u}' = -g\nabla h'$, $\zeta' = \partial v'/\partial x - \partial u'/\partial y$ is the anomalous vorticity, and the term $-\nabla\cdot\overline{\mathbf{u}'\zeta'}$ denotes convergence of eddy vorticity flux. As noted by Hoskins et al. (1983), $-\nabla\cdot\overline{\mathbf{u}'\zeta'}$ is often dominated by small-scale features and it is more informative to consider S by applying the inverse Laplacian operator ∇^{-2} to $-\nabla\cdot\overline{\mathbf{u}'\zeta'}$. Physically, S represents the eddy forcing upon the mean streamfunction, or

[3] Although in situ current measurements are unavailable around the Shatsky Rise, lowered acoustic Doppler current profiler (ADCP) measurements around 142°E southeast of Japan revealed that the KE jet has an equivalent barotropic structure and can reach depths of more than 4,000 m; see Fig. 5 in Qiu (2002) for the ADCP-derived velocity profile.

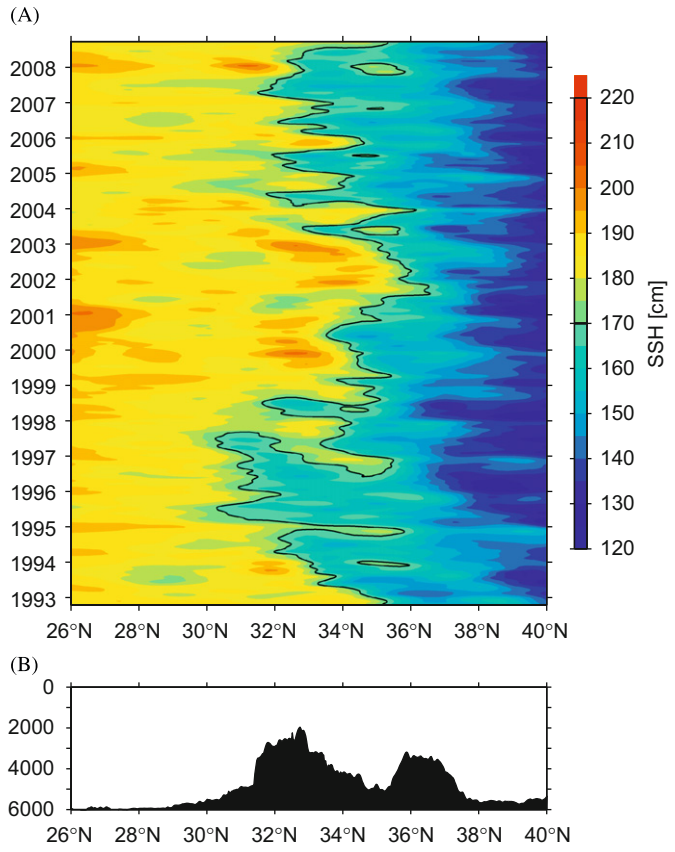

Fig. 7. (A) SSH values averaged downstream of the Shatsky Rise from 162°E to 180°. The black contour denotes the 170-cm isoline, which approximates well the axis of the KE jet. (B) Water depth along 158.2°E where the Shatsky Rise is located (see Fig. 1 A).

SSH, field. A positive (negative) S represents an acceleration of an anticyclonic (cyclonic) circulation.

To emphasize the forcing by mesoscale eddies, we evaluate the time-varying $S(x,y,t)$ field by defining the overbar in Eq. (4) as an average over a one-year period and the prime, the deviation from the annual average. Fig. 8 A shows the spatial pattern of $S_p(x,y)$ after we project the time-varying S field to the normalized time series of the eddy kinetic energy level in the upstream KE region (i.e., Fig. 3 B):

$$S_p(x,y) = \frac{\langle S(x,y,t)E(t)\rangle}{\sqrt{\langle E(t)E(t)\rangle}}. \quad (5)$$

In Eq. (5), angle brackets denote the ensemble average in time and $E(t)$ denotes the eddy kinetic energy time series shown in Fig. 3 B. Instead of showing the $S(x,y,t)$ field in time and space, the $S_p(x,y)$ map provides an efficient way to identify the eddy forcing pattern according to the strength of the regional eddy kinetic energy level. Due to the meandering of the KE jet, the $S_p(x,y)$ pattern in Fig. 8 A appears somewhat patchy; nevertheless, several important features are possible to detect. In particular, there is a general anticyclonic forcing inside the RG south of the upstream KE jet, indicating that the enhanced eddy activity during the unstable state of the KE system works to strengthen the southern RG. This result is in good agreement with the observed changes in the RG strength (see Fig. 3 D): as the eddy activity increases after the KE switches to an unstable state, there is a gradual build-up of the RG strength, and this build-up ceases once the KE returns to a stable state.

Along the path of the meandering KE jet, Fig. 8 A reveals a general tendency for a cyclonic forcing in the trough, and an anticyclonic forcing in the ridge, of the KE's quasi-stationary meanders. Dynamically, this implies that the KE's quasi-stationary meanders are being sustained against dissipation by the eddy forcing. This eddy forcing mechanism supports the modeling result by Hurlburt et al. (1996), but is in contrast to the previous theory by White and McCreary (1976) who regarded the KE's quasi-stationary meanders as being an outcome of standing Rossby lee-waves.

In concluding this section, we note that the $S_p(x,y)$ pattern shown in Fig. 8 A is insensitive to the choice of the basis time series $E(t)$ in Eq. (5). Instead of the eddy kinetic energy level, use of the KE path length time series (i.e., Fig. 3 A) for $E(t)$ produces an $S_p(x,y)$ pattern very similar to Fig. 8 A (see Fig. 8 B). In other words, the $S_p(x,y)$ pattern is set by the collective eddy forcing that modulates on the decadal timescale, rather than by the forcing of particular eddies.

5. Discussions

5.1. PDO versus NPGO forcing

To understand the causes for the SSH signals leading to the decadal transitions of the KE dynamic state, we adopted in Section 3 the linear vorticity model, Eq. (2), and emphasized the wind stress curl forcing relating to the PDOs (recall Fig. 6). Using the same linear vorticity model, Ceballos et al. (2009) have recently argued that it is the NPGO-related wind stress curl forcing that determines the decadal SSH variability in the KE region rather than the PDO forcing. It is worth noting that for the period of 1988 to present relevant to this study (see Fig. 9), the PDO and NPGO indices are correlated with a coefficient $r=-0.29$ between the original monthly time series and $r=-0.51$ between their respective one-year running mean time series (i.e., the dashed line in Fig. 9). To further evaluate the importance of the PDO versus NPGO forcing, we plot in Fig. 10 the lagged correlation coefficient between the observed SSH anomalies shown in Fig. 6 B and the PDO and *negative* NPGO indices as a function of longitude and time lag. At the zero time lag, maximum correlation is found near 164°W, the center of the PDO and NPGO forcing. Although the peak r value is slightly higher in the PDO forcing case ($r>0.8$; Fig. 9 A), the overall differences between the two forcing cases are small. Reflecting the longitudinal propagation of the SSH anomaly signals as baroclinic Rossby waves, the high correlation band in both the PDO and NPGO forcing cases shifts westward as the SSH anomaly signals lag behind the forcing indices.

Within the KE region of 140°−160°E of our interest, the correlation coefficients again have comparable values between the two forcing cases with the maximum $r\simeq 0.6$. One difference between the two cases is that the maximum correlation in the NPGO forcing case occurs at a 3-yr lag (which agrees with the findings by Ceballos et al., 2009), whereas in the PDO forcing case it occurs at a 3.5-yr lag. This lag difference results from the subtle phase differences between the PDO and NPGO time series. From the above analysis, it is fair to state that either the PDO or NPGO index could be used to forecast the observed SSH anomaly signals that lead to the decadal dynamic state change in the KE system. The similarity between the two cases stems from the fact that the PDO- and NPGO-related wind forcing is to a large extent linearly correlated during the 1988 to present period.

5.2. Modes of KE jet intensification and lateral migration

An important findings from the long-term satellite altimeter measurements is that as the PDO- or NPGO-forcing induced SSH

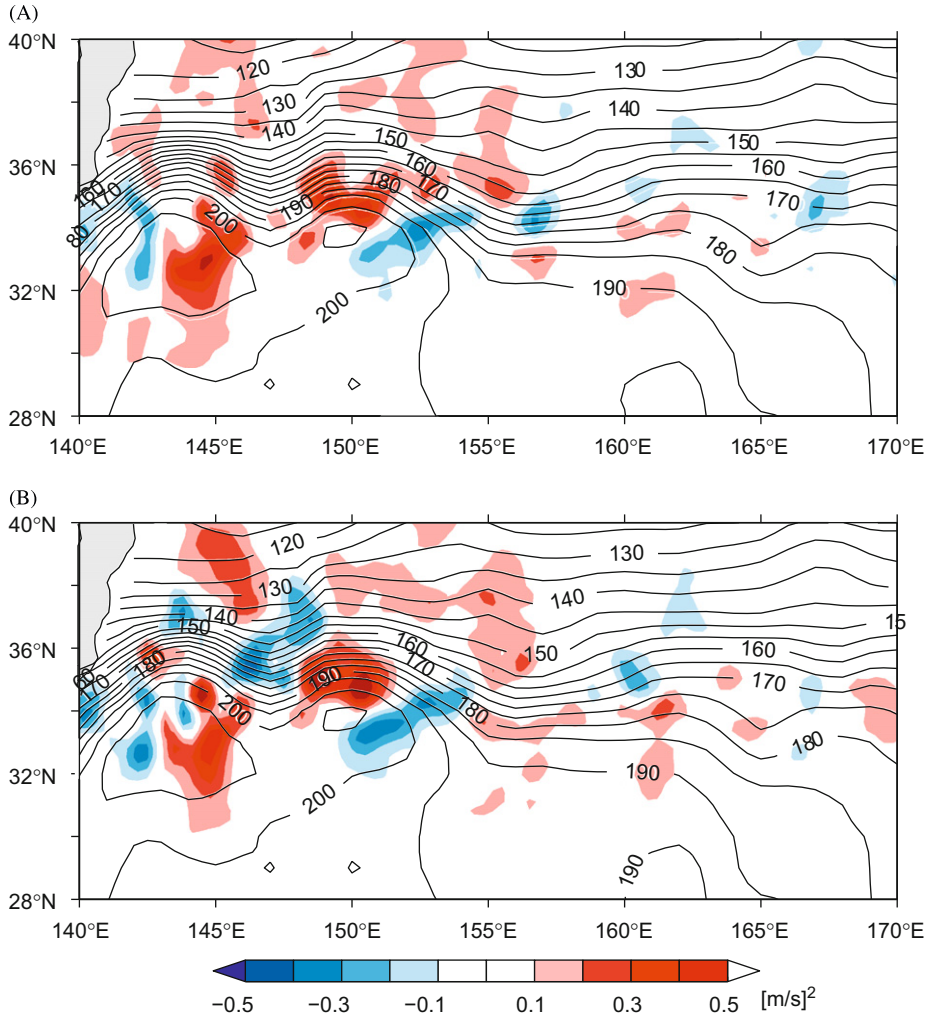

Fig. 8. Eddy-induced acceleration $S_p(x,y)$ of the mean streamfunction field projected to (A) the time series of the level of eddy kinetic energy (i.e. Fig. 3 B) and (B) the time series of the KE path length (i.e. Fig. 3 A). Black contours denote the mean surface dynamic height field (cm) from Teague et al. (1990).

anomalies intrude from the east, both the strength and latitudinal position of the zonal-mean KE jet are simultaneously changed (recall Figs. 3 C and D). Specifically, the KE jet is strengthened and shifted northward when the incoming SSH anomalies are positive and generated by a negative PDO (or positive NPGO) forcing. A cautionary note is that such a *simultaneous* variability of the KE jet can be misinterpreted as two independent modes if an EOF analysis is applied to the SSH anomaly data averaged zonally along the KE jet.

Fig. 11 shows the spatial patterns and their associated PCs of the first two EOF modes after the EOF analysis is applied to the observed $h'(x,y,t)$ data averaged zonally from 142°E to 180°. The first EOF mode explains 42.1% of total variance and represents, judging from the meridional SSH anomaly pattern, the decadal lateral migration change of the zonal-mean KE jet. This mode is identical to the first EOF mode presented in Fig. 2 of Taguchi et al. (2007). Accounting for 21.7% of total variance, the second EOF mode in Fig. 11 has oppositely signed SSH anomaly peaks and represents the strength change of the zonal-mean KE jet. By definition, the two EOF modes are statistically independent and could be interpreted as representing two separate modes associated with the time-varying KE jet. Such an interpretation is clearly inaccurate because the results presented in this study indicate that the observed decadal KE variability is dominated by the concurrent changes in position and strength.

In order to expand this point further, let us consider the case in which an eastward-flowing Gaussian jet is *designed* to fluctuate simultaneously in its strength and position on the decadal time scale:

$$u(y,t)=[A_0+A_1\sin(\omega t)+\sigma_1(t)]\exp\left\{-\frac{[y-y_0-y_1\sin(\omega t+\sigma_2(t))-\sigma_3(t)]^2}{W^2}\right\}, \quad (6)$$

where A_0, y_0, and W denote the amplitude, center latitude, and width of the unperturbed jet, respectively. In (6), $A_1\sin(\omega t)$ signifies the decadally modulating amplitude change of the jet and $y_1\sin(\omega t+\sigma_2(t))$, the jet's decadally modulating position change. By construction, we have assumed that these changes are in phase, except for random fluctuations $\sigma_2(t)$ in the jet's position due to mesoscale eddy signals. To account for additional perturbations by the presence of mesoscale eddies, we have also added random noise $\sigma_1(t)$ and $\sigma_3(t)$ to the jet's amplitude and position in Eq. (6), respectively. Parameter values that are characteristic of the observed time-varying KE jet are: $\omega=2\pi/10$ yr, $A_0=1.0\,\mathrm{m\,s^{-1}}$, $A_1=0.1\,\mathrm{m\,s^{-1}}$, $y_0=35^\circ$N, $y_1=1^\circ$ lat, $W=50$ km, and the white noise amplitudes for σ_1, σ_2, and $\sigma_3=0.1\,\mathrm{m\,s^{-1}}$, $2\pi/5$ yr, and 0.5° lat, respectively.

Using these parameter values and converting $u(y,t)$ to the SSH data allow us to construct a long-term synthetic SSH anomaly

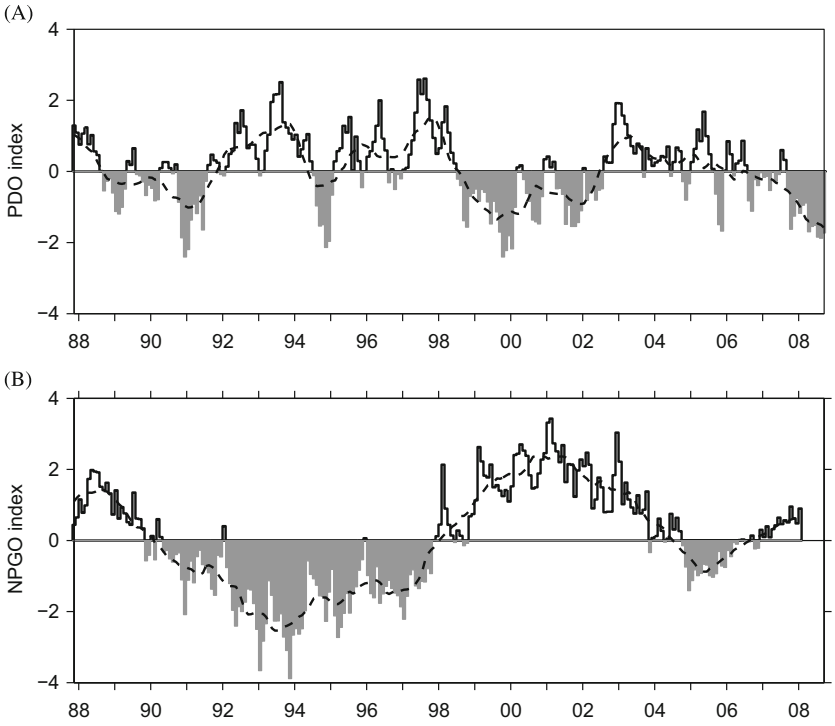

Fig. 9. (A) Monthly Pacific Decadal Oscillation index; same as that shown in Fig. 6 D. (B) Monthly North Pacific Gyre Oscillation index from http://eros.eas.gatech.edu/npgo. In both panels, the dashed line shows the one-year running mean time series.

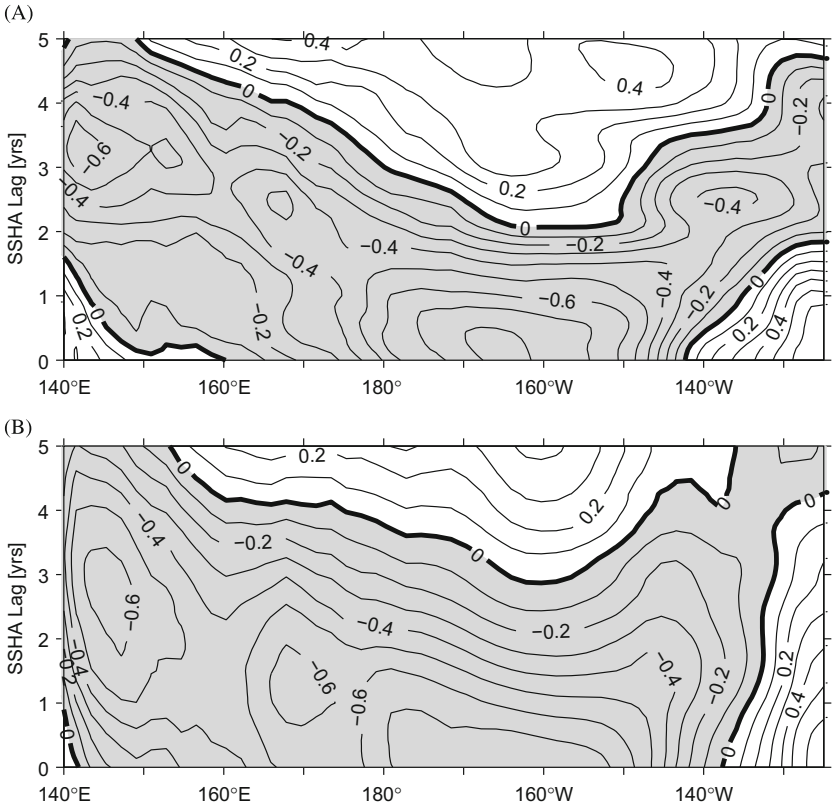

Fig. 10. (A) Lagged correlation between the SSH anomaly data in the zonal band of 32°−34°N (see Fig. 6 B) and the one-year running mean PDO index (Fig. 9 A). (B) Same as (A) except for the negative, one-year running mean NPGO index. Shaded regions indicate negative correlation coefficients.

field. Fig. 12 shows the spatial patterns and their associated PCs of the first two EOF modes from this synthetically constructed SSH anomaly field. Both of the spatial patterns and the PCs bear resemblance to those derived from the observed SSH anomaly data shown in Fig. 11. As in the observed case, it is tempting to interpret the EOF modes in Fig. 12 as representing two separate

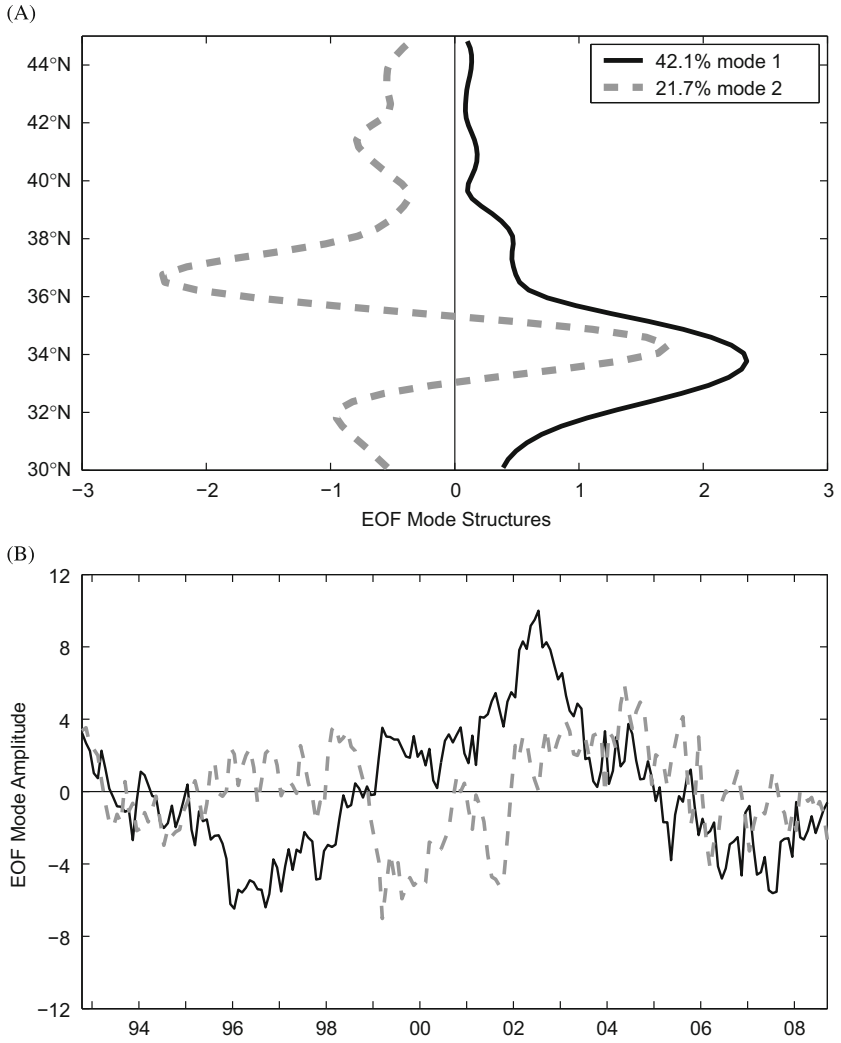

Fig. 11. (A) Spatial patterns and (B) their corresponding principal components of the first two EOF modes for the observed SSH anomaly data averaged zonally from 142°E to 180°. The mean KE jet, as depicted in Fig. 1 A, is located along ~35°N.

modes of the time-varying jet. This interpretation is obviously flawed because there exists, by construction, only one mode of variability in the assumed time-varying jet. The root for this flawed interpretation lies in the fact that it is impossible to use a *single* EOF mode to capture the KE jet that modulates in its amplitude and position simultaneously. In this case, two EOF modes, one representing the amplitude change and the other representing the lateral migration of the jet, will inevitably result. Caution is thus needed in interpreting the modes of the KE variability based on the EOF analysis of observed/modeled SSH anomaly data.

6. Summary

Decadal changes in the Kuroshio Extension (KE) jet, the southern recirculation gyre, and their associated mesoscale eddy signals, are investigated in this study using the satellite altimeter-derived sea surface height data of the past 16 years. The dominant mode of the KE variability is characterized by its oscillations between a stable and an unstable dynamic state. Over the past 16 years, the stable state appeared from late 1992 to mid 1995 and from early 2002 to late 2005, and the unstable state from mid 1995 to late 2001 and from early 2006 to present. In addition to having enhanced eddy kinetic energy level and convoluted paths, the KE jet tends to migrate northward and the southern RG tends to gradually strengthen during the unstable state of the KE system. These tendencies reverse when the KE system shifts to a stable state.

The cause for the bimodal KE oscillations can be sought in the wind stress curl forcing over the eastern North Pacific related to the Pacific decadal oscillations, or the North Pacific Gyre Oscillations. When the PDO (NPGO) index is positive (negative), the Aleutian Low intensifies and shifts southward, generating negative SSH anomalies in the eastern North Pacific through Ekman divergence. As these wind-induced SSH anomalies propagate to the west as baroclinic Rossby waves, they weaken the zonal KE jet and shift its path southward. When the PDO (NPGO) index changes to negative (positive), the enhanced Ekman convergence generates positive SSH anomalies in the east, which enhance the KE jet once they propagate to the west. The importance of the basin-scale wind forcing in initiating the KE's transitions between its two dynamic states was verified in this study using a baroclinic Rossby wave model driven by the NCEP-NCAR reanalysis wind stress data. That the decadal KE variability is largely a forced response to the basin-scale wind forcing, is in

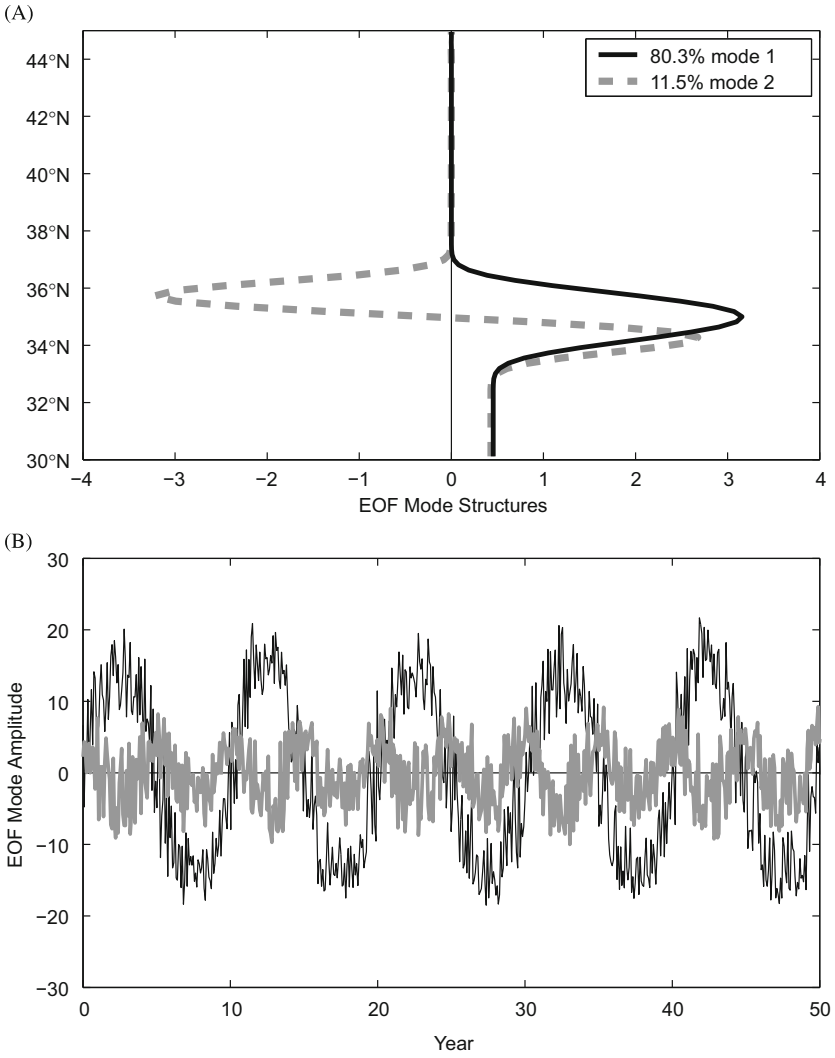

Fig. 12. (A) Spatial patterns and (B) their corresponding principal components of the first two EOF modes for the observed SSH anomaly data averaged zonally from 142°E to 180°. The mean KE jet, as depicted in Fig. 1 A, is located along ~35°N.

contrast to the previous studies that emphasized self-sustained bimodal oscillations in western boundary current extension systems.

The relevance of the linear Rossby wave dynamics in controlling the phase transitions of the KE dynamic state does not negate the important roles played by the nonlinear dynamics. In fact, it is the nonlinear interaction of the deep-reaching KE jet with the Shatsky Rise that determine the level of eddy kinetic energy in the upstream KE region between Japan and the Shatsky Rise. Specifically, as the wind-induced negative SSH anomalies allow the zonal-mean KE jet to migrate southward during a positive (negative) phase of the PDO (NPGO), the deep-reaching KE jet rides over the shallow Shatsky Rise and provides localized disturbations around 158°E that lead to an increase in eddy kinetic energy level during the unstable state of the KE system. In the usptream KE region, the elevated eddy activity during the unstable state of the KE system works to strengthen the southern RG and the meandering quasi-stationary meanders. This gradual strengthening of the southern RG can potentially force the upstream KE path northward and contribute, by combining with the incoming wind-driven positive SSH anomalies from the east, to the KE's transition to a stable dynamic state. It will be interesting for future data analysis and modeling studies to further quantify eddy's feedback upon the mean circulation of the KE system.

Acknowledgments

This study benefited from the discussions with Manu Di Lorenzo, Lee Fu, Art Miller, Stefano Pierini, Niklas Schneider and Bunmei Taguchi. Detailed comments made by an anonymous reviewer helped improve an early version of the manuscript. The surface wind stress data was provided by the National Centers for Environmental Prediction, and the merged satellite altimeter data by the CLS Space Oceanography Division as part of the Environment and Climate EU ENACT project. This research was supported by Contract 1207881 from JPL as part of the NASA Ocean Surface Topography Mission.

References

Adamec, D., 2000. Eddy flow characteristics and mean flow interactions in the North Pacific. Journal of Geophysical Research 105, 11373–11383.

Berloff, P., Hogg, A.M., Dewar, W.K.., 2007. The turbulent oscillator. A mechanism of low-frequency variability of the wind-driven ocean gyres. Journal of Physical Oceanography 37, 2362–2386.

Ceballos, L., Di Lorenzo, E., Hoyos, C.D., Schneider, N., Taguchi, B., 2009. North Pacific gyre oscillation synchronizes climate variability in the eastern and western boundary current systems. Journal of Climate 22, 5163–5174.

Deser, C., Alexander, M.A., Timlin, M.S., 1999. Evidence for a wind driven intensification of the Kuroshio Current Extension from the 1970s to the 1980s. Journal of Climate 12, 1697–1706.

Di Lorenzo, E., Schneider, N., Cobb, K.M., Franks, P.J.S., Chhak, K., Miller, A.J., McWilliams, J.C., Bograd, S.J., Arango, H., Curchister, E., Powell, T.M., Riviere, P., 2008. North Pacific gyre oscillation links ocean climate and ecosystem change. Geophysical Research Letters 35, L08607, doi:10.1029/2007GL032838.

Ducet, N., Le Traon, P.-Y., 2001. A comparison of surface eddy kinetic energy and Reynolds stresses in the Gulf Stream and the Kuroshio Current system from merged TOPEX/Poseidon and ERS-1/2 altimetric data. Journal of Geophysical Research 106, 16603–16662.

Ducet, N., Le Traon, P.-Y., Reverdin, G., 2000. Global high-resolution mapping of ocean circulation from TOPEX/Poseidon and ERS-1 and -2. Journal of Geophysical Research 105, 19477–19498.

Ebuchi, N., Hanawa, K., 2001. Trajectory of mesoscale eddies in the Kuroshio recirculation region. Journal of Oceanography 57, 471–480.

Fu, L.-L., Qiu, B., 2002. Low-frequency variability of the North Pacific Ocean. The roles of boundary- and wind-driven baroclinic Rossby waves. Journal of Geophysical Research 107 doi:10.1029/2001JC001131.

Hogg, A.M., Killworth, P.D., Blundell, J.R., Dewar, W.K., 2005. Mechanisms of decadal variability of the wind-driven ocean circulation. Journal of Physical Oceanography 35, 512–531.

Hoskins, B.J., James, I.J., White, G.J., 1983. The shape, propagation and mean-flow interaction of large-scale weather systems. Journal of Atmospheric Sciences 40, 1595–1612.

Hurlburt, H.E., Wallcraft, A.J., Schmitz, W.J., Hogan, P.J., Metzger, E.J., 1996. Dynamics of the Kuroshio/Oyashio current system using eddy-resolving models of the North Pacific Ocean. Journal of Geophysical Research 101, 941–976.

Ichikawa, K., Imawaki, S., 1994. Life history of a cyclonic ring detached from the Kuroshio Extension as seen by the Geosat altimeter. Journal of Geophysical Research 99, 15953–15966.

Joyce, T.M., Yasuda, I., Hiroe, Y., Komatsu, K., Kawasaki, K., Bahr, F., 2001. Mixing in the meandering Kuroshio Extension and the formation of North Pacific Intermediate Water. Journal of Geophysical Research 106, 4397–4404.

Kistler, R. et al., 2001. The NCEP-NCAR 50-year reanalysis. Monthly means CD-ROM and documentation. Bulletin of the American Meteorological Society 82 , 247–267.

Le Traon, P.-Y., Nadal, F., Ducet, N., 1998. An improved mapping method of multi-satellite altimeter data. Journal of Atmospheric and Oceanic Technology 25, 522–534.

Mantua, N.J., Hare, S.R., Zhang, Y., Wallace, J.M., Francis, R.C., 1997. A Pacific interdecadal climate oscillation with impacts on salmon production. Bulletin of the American Meteorological Society 78, 1069–1079.

Miller, A.J., Cayan, D.R., White, W.B., 1998. A westward-intensified decadal change in the North Pacific thermocline and gyre-scale circulation. Journal of Climate 11, 3112–3127.

Mizuno, K., White, W.B., 1983. Annual and interannual variability in the Kuroshio Current system. Journal of Physical Oceanography 13, 1847–1867.

Pedlosky, J., 1987. Geophysical Fluid Dynamics. Springer, New York.

Pierini, S., 2006. A Kuroshio Extension system model study. Decadal chaotic self-sustained oscillations. Journal of Physical Oceanography 36, 1605–1625.

Primeau, F., 2002. Multiple equilibria and low-frequency variability of the wind-driven ocean circulation. Journal of Physical Oceanography 32, 2236–2256.

Qiu, B., 2002. The Kuroshio Extension system. Its large-scale variability and role in the midlatitude ocean–atmosphere interaction. Journal of Oceanography 58, 57–75.

Qiu, B., 2003. Kuroshio Extension variability and forcing of the Pacific decadal oscillations. Responses and potential feedback. Journal of Physical Oceanography 33, 2465–2482.

Qiu, B., Chen, S., 2005. Variability of the Kuroshio Extension jet, recirculation gyre and mesoscale eddies on decadal timescales. Journal of Physical Oceanography 35, 2090–2103.

Qiu, B., Chen, S., 2006. Decadal variability in the formation of the North Pacific Subtropical Mode Water. Oceanic versus atmospheric control. Journal of Physical Oceanography 36, 1365–1380.

Qiu, B., Chen, S., Hacker, P., 2007. Effect of mesoscale eddies on Subtropical Mode Water variability from the Kuroshio Extension System Study (KESS). Journal of Physical Oceanography 37, 982–1000.

Qiu, B., Kelly, K.A., Joyce, T.M., 1991. Mean flow and variability in the Kuroshio Extension from Geosat altimetry data. Journal of Geophysical Research 96, 18491–18507.

Qiu, B., Miao, W., 2000. Kuroshio path variations south of Japan. Bimodality as a self-sustained internal oscillation. Journal of Physical Oceanography 30, 2124–2137.

Schmeits, M.J., Dijkstra, H.A., 2001. Bimodal behavior of the Kuroshio and the Gulf Stream. Journal of Physical Oceanography 31, 3435–3456.

Schneider, N., Miller, A.J., Pierce, D.W., 2002. Anatomy of North Pacific decadal variability. Journal of Climate 15, 586–605.

Seager, R., Kushnir, Y., Naik, N.H., Cane, M.A., Miller, J., 2001. Wind-driven shifts in the latitude of the Kuroshio–Oyashio extension and generation of SST anomalies on decadal timescales. Journal of Climate 14, 4249–4265.

Smith, W.H.F., Sandwell, D.T., 1994. Bathymetric prediction from dense altimetry and sparse shipboard bathymetry. Journal of Geophysical Research 99, 21803–21824.

Taguchi, B., Xie, S.-P., Schneider, N., Nonaka, M., Sasaki, H., Sasai, Y., 2007. Decadal variability of the Kuroshio extension. Observations and an eddy-resolving model hindcast. Journal of Climate 20, 2357–2377.

Tai, C.-T., White, W.B., 1990. Eddy variability in the Kuroshio extension as revealed by Geosat altimetry. Energy propagation away from the jet, Reynolds stress, and seasonal cycle. Journal of Physical Oceanography 20, 1761–1777.

Teague, W.J., Carron, M.J., Hogan, P.J., 1990. A comparison between the generalized digital environmental model and Levitus climatologies. Journal of Geophysical Research 95, 7167–7183.

Vivier, F., Kelly, K.A., Thompson, L., 2002. Heat budget in the Kuroshio Extension region. 1993–1999. Journal of Physical Oceanography 32, 3436–3454.

White, W.B., McCreary, J.P., 1976. On the formation of the Kuroshio meander and its relationship to the large-scale ocean circulation. Deep-Sea Research 23, 33–47.

Yasuda, I., Okuda, K., Hirai, M., 1992. Evolution of a Kuroshio warm-core ring—variability of the hydrographic structure. Deep-Sea Research 39, 131–161.